

A generic method to constrain the dark matter model parameters from Fermi observations of dwarf spheroidals

Yue-Lin Sming Tsai¹, Qiang Yuan^{2,3}, Xiaoyuan Huang⁴

¹*National Center for Nuclear Research, Hoza 69, 00-681 Warsaw, Poland*

²*Key Laboratory of Particle Astrophysics, Institute of High Energy Physics, Chinese Academy of Sciences, Beijing 100049, P. R. China*

³*Key Laboratory of Dark Matter and Space Astronomy, Purple Mountain Observatory, Chinese Academy of Sciences, Nanjing 210008, P. R. China*

⁴*National Astronomical Observatories, Chinese Academy of Sciences, Beijing 100012, P. R. China*
(Dated: February 24, 2022)

Observation of γ -rays from dwarf galaxies is an effective way to search for particle dark matter. Using 4-year data of Fermi-LAT observations on a series of Milky Way satellites, we develop a general way to search for the signals from dark matter annihilation in such objects. Instead of giving prior information about the energy spectrum of dark matter annihilation, we bin the Fermi-LAT data into several energy bins and build a likelihood map in the “energy bin - flux” plane. The final likelihood of any spectrum can be easily derived through combining the likelihood of all the energy bins. It gives consistent result with that directly calculated using the Fermi Scientific Tool. This method is very efficient for the study of any specific dark matter models with γ -rays. We use the new likelihood map with Fermi-LAT 4 year data to fit the parameter space in three representative dark matter models: i) toy dark matter model, ii) effective dark matter operators, and iii) supersymmetric neutralino dark matter.

PACS numbers: 95.35.+d, 95.85.Pw

I. INTRODUCTION

Detecting particle dark matter (DM) is one of the most important task for the modern physics, although its existence has been revealed through astronomical observations for more than seventy years. The DM particles could annihilate themselves to produce standard model (SM) particles such as electrons/positrons, proton/antiprotons, γ -ray photons and neutrinos, which provides us a chance to detect the DM indirectly in the cosmic radiation. The Fermi Large Area Telescope (Fermi-LAT) is currently the best detector for γ -ray detection in space and could substantially increase the sensitivity for DM search.

The dwarf spheroidal satellites (dSphs) in the Milky Way are generally regarded as ideal candidates when searching for possible DM annihilation signals due to their high DM content and low baryonic contamination. The search for γ -ray emission from dSphs with Fermi-LAT data was performed in many works [1–8]. Without finding any significant “signal” from these targets, stringent upper limits on DM annihilation cross section can be derived. It was shown that for $m_\chi \lesssim 20$ GeV the canonical thermally produced DM with cross section $\sim 3 \times 10^{-26} \text{ cm}^3 \text{ s}^{-1}$ was ruled out with two-year Fermi-LAT observations on 10 dSphs [2] (see also [3] for similar conclusion).

There are usually two ways to extract the limits on DM models from the γ -ray observations. The most con-

servative and DM-model-independent way is to require the DM-induced signal not to exceed the flux/limit of specific source. But in this way, the spectral and spatial information of DM is missing and the constraint is usually weak¹. Another way which could be more realistic is to incorporate the expected γ -ray spectrum and/or the sky map in the analysis. However, it needs to input the model of DM when analyzing the data and is not convenient for generic purpose.

In this work we alternatively adopt a more general way to extract the limits on the γ -ray emission of the dSphs from Fermi-LAT data. The Fermi-LAT observational data are binned into a series of energy bins, and the likelihood in each energy bin is calculated assuming a constant value of the flux from DM annihilation in this energy bin. Given any shape of the γ -ray spectrum, we can easily derive the total likelihood with such a likelihood map on “energy-flux” plane. This method is model-independent in the level of extracting the likelihood of γ -ray flux in each energy bin, and it is more flexible and time-saving to subsequently discuss any kind of particle models. The detailed description of the method is given in Sec. II. In Sec. III we apply this method to several

¹ Note in [6] a stronger constraint was given. In that work a lower upper limit of γ -ray flux was derived through subtracting the photon counts of chosen “background” region from the “signal” region.

DM models.

II. LIKELIHOOD MAP

In this section, we will describe the methodology of how to build a particle model-independent likelihood map. The γ -ray flux from annihilation of DM in a dSph is

$$\phi(E) = \frac{\langle\sigma v\rangle}{8\pi m_\chi^2} \times \frac{dN_\gamma}{dE_\gamma} \times J, \quad (1)$$

where m_χ is the mass of DM particle, $\langle\sigma v\rangle$ is the average velocity-weighted annihilation cross section, $\frac{dN_\gamma}{dE_\gamma}$ is the γ -ray yield spectrum of one annihilation of a DM pair, and $J = \int dl d\Omega \rho^2(l)$ is the integral density square of DM.

From Fermi-LAT 2-year result [2], we can see $\langle\sigma v\rangle$ with the $b\bar{b}$ channel for $m_\chi \lesssim 25$ GeV is lower than the result expected from thermal equilibrium, $\langle\sigma v\rangle \sim 3 \times 10^{-26} \text{ cm}^3 \text{ s}^{-1}$. It could be a hint that Fermi-LAT can rule out DM annihilation to $b\bar{b}$, at least, at the lower mass region, $m_\chi \lesssim 25$ GeV. However, the above information cannot be true for realistic DM models. In most of particle models such as supersymmetry (SUSY), γ -rays can be produced via several annihilation channels. Moreover, $\frac{dN_\gamma}{dE_\gamma}$ can differ from one point to another in the SUSY parameter space. Therefore it will be more useful to have a likelihood map which does not depend on a pre-determined $\frac{dN_\gamma}{dE_\gamma}$. To do so, we bin the photons into small energy bins $[E_i, E_{i+1}]$, and assume the differential energy spectrum $\frac{dN_\gamma}{dE_\gamma}$ in the small energy interval to be constant C_i . Then the likelihood is built based on two new variables, E_i and $\phi_{ij} = \frac{\langle\sigma v\rangle}{8\pi m_\chi^2} \times C_i \times J_j$, where i is the index of energy bin and j is the index of individual dSph. We adopt the same 10 dSphs in this study as in [2].

To calculate the likelihood from Fermi-LAT data we employ 4-year Fermi-LAT data² recorded from 4 August 2008 to 2 August 2012, with the pass 7 photon selection. The LAT Scientific Tools version v9r27p1 are used for the analysis. The “SOURCE” (evclass=2) event class is selected, and the recommended filter cut “(DATA_QUAL==1) && (LAT_CONFIG==1) && ABS(ROCK_ANGLE)< 52” is applied. The photon energy range is chosen from 200 MeV to 200 GeV, and the region-of-interest (ROI) is adopted to be a $14^\circ \times 14^\circ$ box centered around the center of each dSph. The instrument response function used is “P7SOURCE_V6”. For the

diffuse background, we use the Galactic diffuse model `gal_2yearp7v6_v0.fits` and the isotropic diffuse spectrum `iso_p7v6source.txt` provided by the Fermi Science Support Center³. The point sources of the second LAT source catalog are also included in the modeling [9]. The binned likelihood method is used to calculate the likelihood L_{ij}^{LAT} . The DM contribution is modelled as a point source located at the central position of each dSph. In the analysis the free parameters include all the normalizations of the second LAT sources in the ROI, and the normalizations of the two diffuse backgrounds.

We follow the method described in [2] to combine the results of different dSphs. Note that J_j factor is absorbed in ϕ_{ij} when calculating L_{ij}^{LAT} . To get rid of the effect of J_j , we define

$$\psi_i = \phi_{ij}/J_j = \frac{\langle\sigma v\rangle}{8\pi m_\chi^2} \times C_i, \quad (2)$$

and write the joint likelihood function as

$$L_i(D|\psi_i) = \prod_j L_{ij}^{\text{LAT}}(D|\psi_i, \mathbf{p}_j) \times \frac{1}{\ln(10) J_j \sqrt{2\pi} \sigma_j} e^{-[\log_{10}(J_j) - \overline{\log_{10}(J_j)}]^2 / 2\sigma_j^2}, \quad (3)$$

where D represents the binned γ -ray data and $\{\mathbf{p}\}_j$ are the ROI-dependent model parameters. $\overline{\log_{10}(J_j)}$ and σ_j are the mean and standard deviations of the Gaussian distribution of $\log_{10}(J_j)$. It is worth pointing out that the J -factors are weakly dependent on the density profile of the halo. Taking Draco as an example, the J factor for Burkert profile [4] according to the stellar kinematics [10] is similar with that for NFW profile as given in [2]. Moreover, the authors of Ref. [11] perform a scan with five halo parameters varied. Interestingly, they found that the highly cuspy NFW profile and a flat isothermal core profile could fit the data equally well and the posterior distribution of J was still similar with the value given in [2]. In this work we take the values of J -factors and the uncertainties from Table I of [2].

We perform a grid scan with 10 energy bins logarithmically spaced between 0.2 and 200 GeV, and 50 bins of ψ_i logarithmically spaced from 10^{-33} to $10^{-25} \text{ cm}^3 \text{ s}^{-1} \text{ GeV}^{-3}$. For each given (E_i, ψ_i) point, we vary all the nuisance parameters as well as J_i , known as the “profile likelihood” technique [12], and take the maximum likelihood of Eq. (3) as the final likelihood probability value. The combined likelihood map based on E_i and $E_i^2 \psi_i$ is shown

² <http://fermi.gsfc.nasa.gov/ssc/data>

³ <http://fermi.gsfc.nasa.gov/ssc/data/access/lat/Background-Models.html>

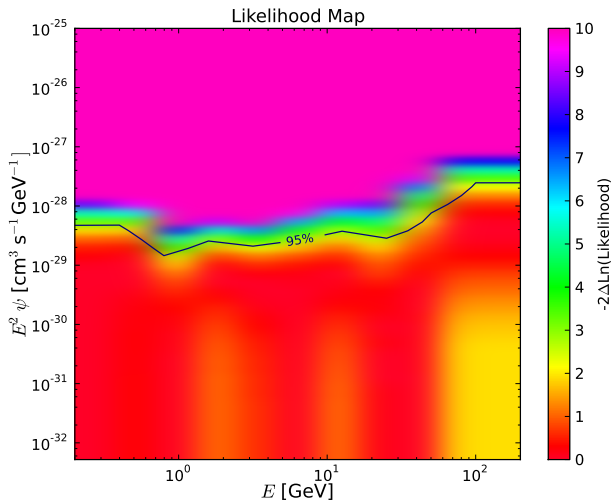


FIG. 1: The likelihood map on $(E_\gamma, E_\gamma^2 \psi)$ plane based on 4-year Fermi-LAT data on the 10 dSphs. The black solid line is one-sided 95% exclusion limit. The color shows the value of $-2\Delta \ln \mathcal{L}$ with the likelihood normalized in each energy bin.

in Fig. 1. For each energy bin, we normalize the maximum likelihood to one. The solid line is a one-sided 95% confidence level, corresponding to $-2\Delta \ln \mathcal{L} = 2.71$. One should bear in mind that these limits shown in Fig. 1 are totally independent of the theoretical model parameters of DM, such as m_χ , $\langle \sigma v \rangle$, and $\frac{dN_\gamma}{dE_\gamma}$. It indicates that any expected γ -ray flux should not exceed the limits in the whole energy range from 0.2 GeV to 200 GeV. However, such a requirement is too conservative compared with the combined likelihood of all energy bins (see the next paragraph). If one wants to discuss the specific models of the γ -ray emission and derive the constraints on the specific model parameters such as $(m_\chi, \langle \sigma v \rangle)$ of DM annihilation, the spectral information will be required. However, such a likelihood map in $(m_\chi, \langle \sigma v \rangle)$ plane is $\frac{dN_\gamma}{dE_\gamma}$ dependent.

Combining the likelihood of each energy bin we can get the total likelihood for any input spectrum $\frac{dN_\gamma}{dE_\gamma}$. The total likelihood can be calculated as

$$L = \prod_i L_i(D|\psi_i), \quad (4)$$

where ψ_i is the expected flux of the spectrum in the i th energy bin, with $C_i \approx \frac{dN_\gamma}{dE_\gamma} \bigg|_{\sqrt{E_i E_{i+1}}}$. Inserting Eq. (2) to (4), one can translate the likelihood map from (E_i, ψ_i) plane (Fig. 1) to $(m_\chi, \langle \sigma v \rangle)$ plane. As mentioned above, the likelihood map in $(m_\chi, \langle \sigma v \rangle)$ plane will depend on the spectrum $\frac{dN_\gamma}{dE_\gamma}$.

At the level of detailed DM model, m_χ , $\langle \sigma v \rangle$ and $\frac{dN_\gamma}{dE_\gamma}$ are variable with other intrinsic parameters of the model. With the above likelihood map (Fig. 1), we can eas-

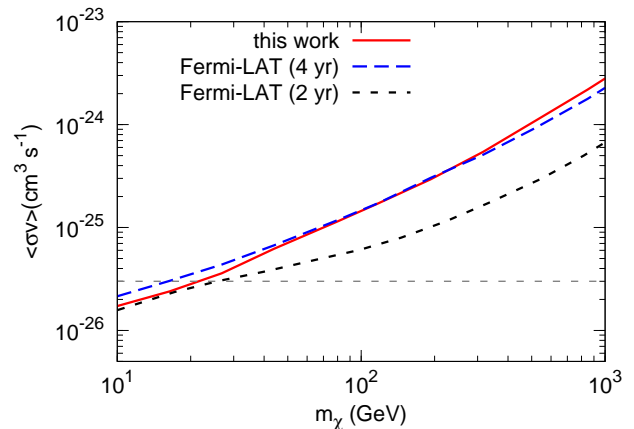


FIG. 2: Comparison of the results using the likelihood map method developed in this work (solid) and that derived using Fermi Scientific Tool (long dashed). Here we assume $b\bar{b}$ channel of DM annihilation and the results from the ten dSphs are combined. The 2-year result from [2] is also shown.

ily find the likelihood of any set of DM parameters. Of course, for each model point one can implement the output γ -ray spectrum in the `Fermi Scientific tools` and calculate its likelihood. But it will be much more computing time-consuming compared with our method.

In Fig. 2 we give the comparison of our result with that derived using the Fermi tool (following directly the way in [2] but using 4-yr data), for DM annihilation to $b\bar{b}$ channel. We can see that these two results agree well with each other. Also the two-year result given in [2] is shown. The results show that the 4-yr constraint is even weaker than that of 2-yr constraint. Similar result was also reported recently [13], and it was possibly due to the update to pass 7 of the data and the statistical fluctuations. One should not be confused with the 95% upper limit in Fig. 2 and Fig. 1. The line in Fig. 1 is 95% upper limit of $E_i^2 \psi_i$ at given γ -ray energy bin, while the line in Fig. 2 is 95% upper limit of $\langle \sigma v \rangle$ at given m_χ based on total likelihood for γ -rays from 0.2 to 200 GeV. A model point disfavoured by likelihood at some certain energy bin must be also ruled out by the total likelihood. On the contrast, a model point disfavoured by the total likelihood function does not mean that it is necessarily ruled out by the 95% line of Fig. 1.

III. PARTICLE MODEL FIT

In this section we apply the method described in Sec. II to specific DM models to derive the constraints. Three particle models, a toy model, the effective DM model, and the supersymmetry neutralino DM are adopted as

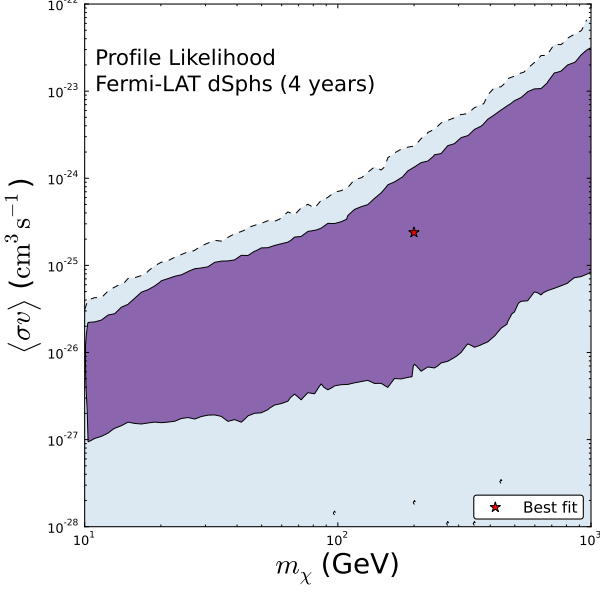


FIG. 3: The 68% (inner) and 95% (outer) profile likelihood contour for the toy model.

examples.

A. Toy model

To generalize the upper limit on $m_\chi - \langle\sigma v\rangle$ plane, we design a toy DM model which annihilates to γ -rays only via $b\bar{b}$, $\tau^+\tau^-$, and W^+W^- channels. We only consider these three channels because the differences between them are relatively large compared with other channels.

With the 4-year likelihood map (Fig. 1), we conduct a random scan of the four parameters, m_χ , $\langle\sigma v\rangle_{b\bar{b}}$, $\langle\sigma v\rangle_{\tau^+\tau^-}$, and $\langle\sigma v\rangle_{W^+W^-}$. The total cross section $\langle\sigma v\rangle$ equals to the sum of the three channels. The best-fit point obtained in the scan is: $m_\chi = 200$ GeV, $\langle\sigma v\rangle = 2.39 \times 10^{-25} \text{cm}^3 \text{s}^{-1}$, $\text{BR}_{b\bar{b}} = 0.47$, $\text{BR}_{\tau^+\tau^-} = 0.53$, and $\text{BR}_{W^+W^-} = 10^{-3}$. Not surprisingly, the mixed channels can give better fit due to more degrees of freedom. However, the current Fermi-LAT data can not effectively constrain the branching ratios, namely the shapes of $\frac{dN_\gamma}{dE_\gamma}$.

In Fig. 3, we present 68% (inner) and 95% (outer) contours on the $m_\chi - \langle\sigma v\rangle$ using the profile likelihood method. Since we project the model parameter space from 4 to 2 variables, the 68% and 95% contours are defined with $\int_R L(D|m_\chi, \langle\sigma v\rangle) dm_\chi d\langle\sigma v\rangle$ equals to 0.68 and 0.95, respectively. Here, R is the region within the contours. Compared with Fig. 2, we can clearly see that the 95% upper limit of this toy model is significantly higher than that of $b\bar{b}$ channel only for $m_\chi \gtrsim 100$ GeV

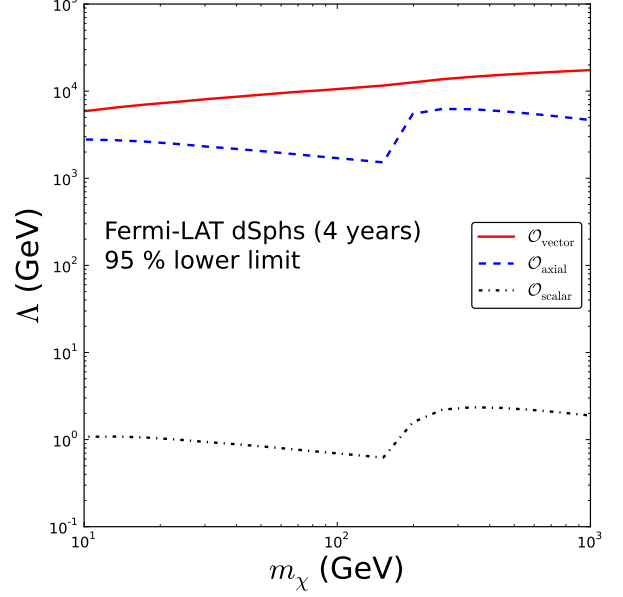


FIG. 4: The 95% lower limits on Λ for each operator from the 4-year Fermi-LAT dSph data.

and slightly higher for lower masses. This is because of the inclusion of $\tau^+\tau^-$ channel in the toy model. According to the results in [2], for $m_\chi \lesssim 100$ GeV the constraints on $\langle\sigma v\rangle_{b\bar{b}}$ and $\langle\sigma v\rangle_{\tau^+\tau^-}$ are comparable, while for higher DM mass the constraint on $\langle\sigma v\rangle_{\tau^+\tau^-}$ becomes much weaker than that on $\langle\sigma v\rangle_{b\bar{b}}$. Including W^+W^- channel also makes the total constraint weaker.

B. Effective DM models

Before assuming particular DM models, we may adopt an effective interaction approach to describe the interactions of the DM particle with the SM particles [14–19]. In such scenario, the DM particle exists in a hidden sector, which communicates with the SM sector via a heavy degree of freedom in the connector sector. At energy scale well below this heavy mediator we can introduce a new energy scales Λ to describe the effective couplings between DM and SM fermions. In this study, we consider the interactions between fermionic DM field χ and SM fermion f described by scalar ($\mathcal{O}_{\text{scalar}}$), vector ($\mathcal{O}_{\text{vector}}$)

or axial ($\mathcal{O}_{\text{axial}}$) operators

$$\mathcal{O}_{\text{vector}} = \sum_f \frac{C_V^f}{\Lambda_V^2} (\bar{\chi} \gamma^\mu \chi) (\bar{f} \gamma_\mu f) , \quad (5)$$

$$\mathcal{O}_{\text{axial}} = \sum_f \frac{C_A^f}{\Lambda_A^2} (\bar{\chi} \gamma^\mu \gamma^5 \chi) (\bar{f} \gamma_\mu \gamma^5 f) , \quad (6)$$

$$\mathcal{O}_{\text{scalar}} = \sum_f \frac{C_S^f m_f}{\Lambda_S^3} (\bar{\chi} \chi) (\bar{f} f) , \quad (7)$$

where $C_{i=V,A,S}$ is an effective coupling constant of order \mathcal{O} that can be absorbed into Λ_i and f runs over all the lepton and quark states. Except $\mathcal{O}_{\text{scalar}}$ whose coupling also depends on m_f , $\mathcal{O}_{\text{vector}}$ and $\mathcal{O}_{\text{axial}}$ both have universal coupling to all the fermions.

We follow the calculation in [18] to obtain $\langle \sigma v \rangle$ and $\frac{dN_\gamma}{dE_\gamma}$ for the effective DM models, and constrain each of the effective operators using the 4-year Fermi-LAT dSph data. Since we assume a universal coupling for all the fermions and the top quark channel only opens at $m_\chi > 172$ GeV, the upper limits of $\langle \sigma v \rangle$ of these three operators at low mass region $m_\chi < 172$ GeV behave like $b\bar{b}$ channel in Fig. 2. Even if the $t\bar{t}$ channel opens, due to the large contribution to the γ -ray flux through the $b\bar{b}$ channel, the result is still not much different from the one $\chi\chi$ directly to the $b\bar{b}$. However, it is worthy to mention that the constraints on $\langle \sigma v \rangle$ of the three operators will depend on m_f (see Eqs. (A1), (A4) and (A7) in [18]).

In Fig. 4, we show the 95% lower limits on (m_χ, Λ) plane for operators $\mathcal{O}_{\text{scalar}}$ (black dash-dotted), $\mathcal{O}_{\text{vector}}$ (red solid) and $\mathcal{O}_{\text{axial}}$ (blue dashed) and $\mathcal{O}_{\text{scalar}}$. It is clear to see that both $\mathcal{O}_{\text{axial}}$ and $\mathcal{O}_{\text{scalar}}$ have a kink at the top quark mass because the $t\bar{t}$ channel opens. For operator $\mathcal{O}_{\text{vector}}$ there is only a very weak dependence on m_f , and the $t\bar{t}$ channel is suppressed.

It is of interest to compare the limit on (m_χ, Λ) plane driven by the Fermi-LAT gamma-ray low-latitude result [18] and our dSphs lower limits. The limits from dSphs for all three operators are slightly stronger. However, comparing our result with the one obtained from Galactic radio [19], we found that the constraint for $\mathcal{O}_{\text{vector}}$ from dSphs can be stronger than the Galactic radio.

C. The Minimal Supersymmetric Standard Model

Undoubtedly, among various particle physics models, SUSY neutralino is the most popular DM candidate. However, many recent published results such as a Higgs boson candidate discovery at the LHC, flavour physics, $\delta(g-2)_\mu$ (the muon's anomalous magnetic moment), and the relic density of DM can set strong constraints on the SUSY parameter space. In addition, Fermi-LAT γ ray

data can also test the SUSY DM, e.g., the minimal supersymmetric standard model (MSSM) [20, 21] and the Constrained MSSM [22, 23]. In this subsection, we use 4-year Fermi data on dSphs to test the MSSM scenario of DM.

Given the large number of parameters in the MSSM, we have to take some reasonable and simplified assumptions. We start by assuming that no CP violating phases are present, and that all mass matrices and trilinear couplings are diagonal in flavor space, in order not to violate the quite stringent constraints on flavor changing neutral currents (FCNCs). Moreover, we take the first and second generations of scalars to be degenerate, again motivated by experimental constraints, such as $K - \bar{K}$ mixing. As the trilinears are proportional to the fermion masses, we can safely ignore the contributions from the first and second generations as they are dwarfed by the third generation.

Unless there is a lighter gravitino or R-parity is not conserved, the lightest neutralino is the only MSSM particle that can make a good DM candidate. The lightest neutralino is the lightest mass eigenstate of a mixed gauge-eigenstate, Bino, Wino, up-type Higgsino, and down-type Higgsino,

$$\chi_1^0 = Z_{\text{bino}} \tilde{B} + Z_{\text{wino}} \tilde{W} + Z_{H_u} \tilde{H}_u + Z_{H_d} \tilde{H}_d. \quad (8)$$

The coefficients Z_i ($i = \text{bino, wino, } H_u, H_d$) are determined by diagonalizing the neutralino mass matrix. To describe the neutralino compositions, it is convenient to introduce a gaugino fraction, $f_g = Z_{\text{bino}}^2 / (Z_{\text{bino}}^2 + Z_{\text{wino}}^2)$. When f_g is close to 1, gauginos will dominate the neutralino, on the other hand the neutralino will be higgsino-like if $f_g \sim 0$.

The input parameters and their prior ranges are shown in Table I. After the Higgs candidate was discovered at the LHC [24, 25], the Higgs resonance region, $2m_\chi \sim m_h \sim 126$ GeV, can drive a large γ -ray flux because of small m_χ and large $\langle \sigma v \rangle$. Besides the Higgs resonance region, one can also have a large ψ_i at the Focus point region and A-funnel region with small m_χ . We let $m_1 = 0.5m_2$ to obtain a bino-like neutralino. However, we still allow a Higgsino like neutralino, particularly at $m_\chi \sim 1$ TeV, which is strongly disfavoured by $\delta(g-2)_\mu$ constraint. We keep the 1st and 2nd generations of squarks as heavy as ~ 2.5 TeV and the first two generations of slepton masses $m_{\tilde{L}_{1,2}} = m_1 + 50$ GeV at SUSY scale.

To conduct the investigation, we use the nested sampling algorithm, implemented in **MultiNest**[26] which is incorporated into **BayesFITS** package, with 9000 live points, evidence tolerance factor 0.5, and sampling efficiency 0.8. To get rid of prior dependence and evenly explore the full parameter space, we make two separate

Parameter	Range
bino mass (GeV)	$m_1 = 0.5m_2$
wino mass (GeV)	$10 < m_2 < 4 \times 10^3$
gluino mass (TeV)	$0.7 < m_3 < 5$
top/ τ -quark trilinear (TeV)	$-7 < A_t, A_\tau < 7$
b-quark trilinear (TeV)	$A_b = 0.5$
pseudoscalar mass (TeV)	$0.2 < m_A < 4$
μ parameter (TeV)	$10^{-2} < \mu < 4$
3rd gen. squark mass (TeV)	$0.3 < m_{\tilde{Q}_3} < 4$
stau mass (TeV)	$0.1 < m_{\tilde{\tau}} < 4$
1st/2nd gen. slepton mass (GeV)	$m_{\tilde{L}_{1,2}} = m_1 + 50$
1st/2nd gen. squark mass (TeV)	$m_{\tilde{Q}_{1,2}} = 2.5$
ratio of Higgs doublet VEVs	$3 < \tan \beta < 62$

TABLE I: The prior ranges of input parameters over which we perform the scan of the MSSM. We make two separate scans, one with flat priors and the other one with log priors for all mass parameters. In both scans, we adopt a flat prior for $\tan \beta$ and trilinear couplings.

runs, one with flat priors and the other with log priors for all the mass parameters. For the rest parameters we use only the flat priors. The observables included in the total likelihood $\mathcal{L}_{\text{total}}$ used to constrain the parameter space are Higgs mass $m_h \sim 126$ GeV, WMAP relic density $\Omega_\chi h^2$, $B_s \rightarrow \mu^+ \mu^-$, $b \rightarrow s \gamma$, $B_u \rightarrow \tau \nu$, and ΔM_{B_s} . For SM precision, we also include m_W and $\sin \theta_{\text{eff}}$. The theoretical and experimental errors can be found in Ref. [27] and references therein. Regarding to the relic density we assume that there is no other DM ingredients except neutralino. If the relic density is not dominant by neutralino, the DM fluxes must be rescaled by a factor $(\Omega_\chi / \Omega_{\text{WMAP}})^2$ because of DM densities. We are only interested that $\mathcal{L}_{\text{dSphs}}$ is improved by adding the rescaling factor but ψ_i is still large enough to be detectable by Fermi-LAT. To obtain the above solution, it is only possible that Ω_χ is slightly smaller than Ω_{WMAP} . Therefore, in the level of scan, we will only consider a Gaussian likelihood instead of an upper limit for neutralino relic density. In addition, we also check the exclusion bounds obtained from the Higgs searches at LEP and the Tevatron, by implementing **HiggsBounds-3.8.0** [28]. Note that we do not use $\delta(g-2)_\mu$ constraint because it strongly disfavoured for $m_\chi \gtrsim 600$ GeV where neutralino is most Higgsino-like.

The total γ -ray spectrum from neutralino annihilation is given by

$$\frac{dN_\gamma}{dE_\gamma} = \sum_f \sum_X B_f \frac{dN_f^\gamma(X)}{dE}, \quad (9)$$

where X runs over the contributions of secondary photons, final state radiation, virtual internal

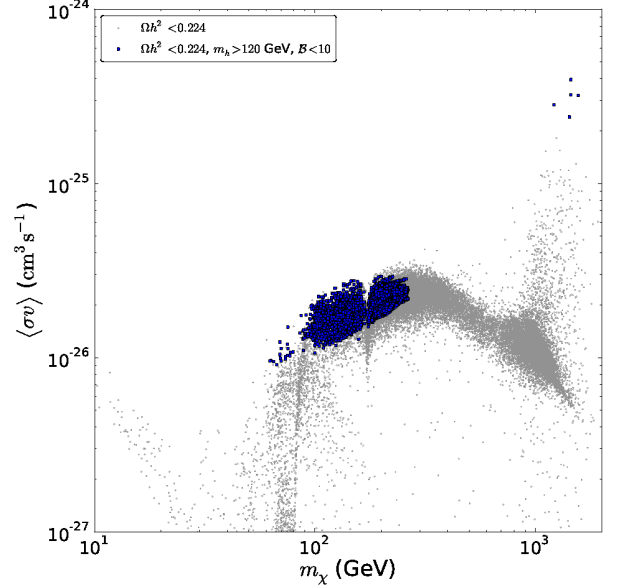


FIG. 5: The impact of 4-year Fermi-LAT dSph result on $(m_\chi, \langle \sigma v \rangle)$ plane of neutralino DM. The grey dots satisfy $\Omega h^2 < 0.224$ and $-2 \ln \mathcal{L}_{\text{total}} < 20$, and the blue squares are selected from grey cycle points with $m_h > 120$ GeV and $\mathcal{B} < 10$.

bremsstrahlung, and monochromatic γ -ray line, B_f is the branching ratio into the annihilation channel f . The contribution from secondary photons is mainly produced through the decay of π^0 and K^0 . For completeness, we also include the monochromatic γ -ray line contributions because $\chi\chi \rightarrow \gamma\gamma/\gamma Z$ can slightly contribute to our likelihood for $m_\chi \lesssim 200$ GeV. The spectrum is calculated using the **DarkSUSY-5.0.6** package [29].

It is possible that the annihilation cross section of DM in the Milky Way today can be boosted by non-perturbative Sommerfeld corrections compared with that in the early Universe, especially for $m_\chi \gtrsim \text{TeV}$ in the MSSM case (e.g., [30–32]). In the MSSM, the lightest neutralino with mass $\sim \text{TeV}$ are mostly Wino- or Higgsino-like, with Sommerfeld enhancement factor of order $O(1)$ [30–32]. On the other hand, $\frac{dN_\gamma}{dE_\gamma}$ can differ by a factor of several between different simulation codes **Pythia6** [33], **Pythia8** [34] and **Herwig** [35]. To investigate possible source of boost factor which could come from either the Sommerfeld enhancement or uncertainties of $\frac{dN_\gamma}{dE_\gamma}$, we can employ a phenomenological boost factor \mathcal{B} to boost our SUSY prediction flux ψ_i^{SUSY} in order to obtain the maximum dSphs likelihood, $\psi_i(\mathcal{L}_{\text{max}}^{\text{dSphs}}) = \mathcal{B} \psi_i^{\text{SUSY}}$.

We present the scan result on $(m_\chi, \langle \sigma v \rangle)$ plane in

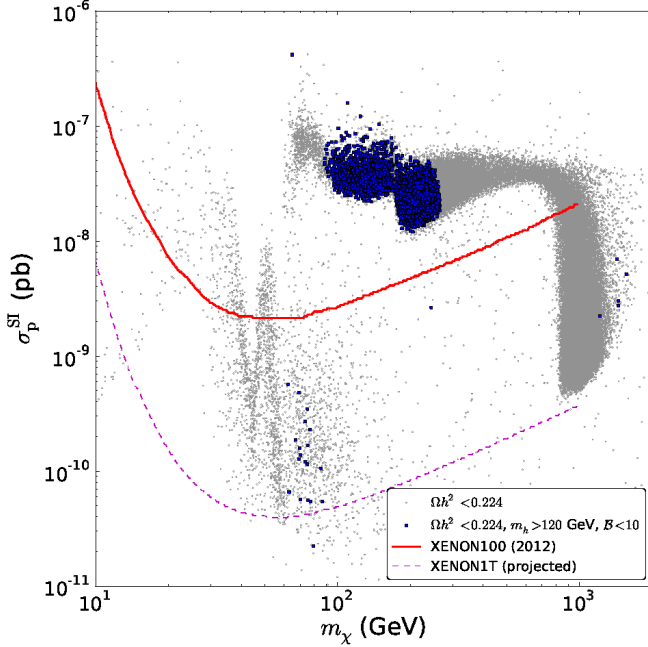


FIG. 6: The scatter plot on the $(m_\chi, \sigma_p^{\text{SI}})$ plane in the MSSM. The color scheme is same as Fig. 5. The solid (red) line is XENON100 (2012) 95% upper limit and the dashed (magenta) line is XENON1T projected sensitivity.

Fig. 5. Totally $\sim 200,000$ sample points are obtained. The grey dots correspond to the sample surviving from $-\ln \mathcal{L}_{\text{total}} < 20$ and $\Omega h^2 < 0.224$ cut. From Ref. [32], we can see Sommerfeld corrections can also reduce the relic density. Since we do not include the Sommerfeld corrections in our relic density computation, we here apply a broader range $\Omega h^2 < 2\Omega_{\text{WMAP}} h^2$ cut in order to conservatively include the possible points. The blue squares are selected from the grey dots with criteria $m_h > 120$ and $\mathcal{B} < 10$. We find that the blue squares for $m_\chi < 300$ GeV are mostly bino-like neutralino but for $m_\chi > 1200$ GeV they are mostly Higgsino-like neutralino. For those Higgsino-like neutralino the boost factor is found to be $\mathcal{B} \sim 4$, which could be due to either the Sommerfeld effect or the uncertainties of $\frac{dN_\gamma}{dE_\gamma}$. For the bino-like neutralino with lower masses, few points are found with $\mathcal{B} \lesssim 4$. Since the Sommerfeld effect does not apply on such small DM mass range and the uncertainty of $\frac{dN_\gamma}{dE_\gamma}$ is also only a factor of several, we conclude that the 4-year Fermi-LAT data is less sensitive to bino-like than Higgsino-like neutralino.

The constraint on the spin-independent cross section between DM particle and nucleon σ_p^{SI} is shown in Fig. 6. Also shown are the XENON100 (2012) result of the direct detection experiment [36] and the expected sen-

sitivity of XENON1T. We notice that XENON100 can exclude most of neutralinos which have gaugino fraction, $0.6 < f_g < 0.9$. However, for pure gaugino $f_g \sim 1$ or Higgsino $f_g \sim 0$, Fermi-LAT data still can test them prior to XENON1T.

IV. SUMMARY

In this work we develop a generic method to ensure fast computation of the likelihood of any spectral component from Fermi-LAT observations of dSphs. The Fermi-LAT data of each ROI are binned into several energy bins and the likelihood of a point source contribution located at the ROI center in each energy bin is calculated with the public Fermi Scientific Tool. A likelihood map which depends only on the Fermi-LAT data can be derived without the speculated energy spectrum of the new component (Fig. 1). Combining the likelihood of each energy bin we can get the total likelihood of any given energy spectrum. This method is tested to be in good agreement with the results directly derived with Fermi Scientific Tool. It is thought to be of great convenient for the search for DM signals from the Fermi-LAT data, especially for the discussion of specific DM models.

We apply such a method on several DM models, including a toy model with mixture of several channels, the effective operator scenarios and the MSSM models. The Fermi-LAT data can give interesting constraints on the DM models. First, in our toy model fit, we found that the current Fermi-LAT data cannot effectively constrain the shapes of $\frac{dN_\gamma}{dE_\gamma}$. Second, the Fermi-LAT data can improve the lower limits of three effective operators on (m_χ, Λ) plane. Finally, for the MSSM, we find the Fermi-LAT data are more sensitive for the Higgsino-like neutralinos than the bino-like neutralinos. Furthermore, Fermi-LAT data can even test the MSSM models with pure gaugino or Higgsino compositions more effectively than the current direct detection experiments.

The data of the likelihood map and a FORTRAN code [37] to calculate the final likelihood of any input spectral function are provided for download.

Acknowledgments

The authors want to thank Christoph Weniger for very useful discussions of Fermi-LAT dSphs data. YST would like to thank Enrico Sessolo, Leszek Roszkowski and Xiao-Jun Bi for the comments on the SUSY model.

This work is supported by National Natural Science Foundation of China under Grant No. 11105155. QY acknowledges the support from the Key Laboratory of

Dark Matter and Space Astronomy of Chinese Academy of Sciences. YST was funded in part by the Welcome

Programme of the Foundation for Polish Science.

-
- [1] A. A. Abdo *et al.* [Fermi-LAT Collaboration], *Astrophys. J.* **712**, 147 (2010) [arXiv:1001.4531 [astro-ph.CO]].
 - [2] M. Ackermann *et al.* [Fermi-LAT Collaboration], *Phys. Rev. Lett.* **107**, 241302 (2011) [arXiv:1108.3546 [astro-ph.HE]].
 - [3] A. Geringer-Sameth and S. M. Koushiappas, *Phys. Rev. Lett.* **107**, 241303 (2011) [arXiv:1108.2914 [astro-ph.CO]].
 - [4] I. Cholis and P. Salucci, *Phys. Rev. D* **86**, 023528 (2012) [arXiv:1203.2954 [astro-ph.HE]].
 - [5] A. Geringer-Sameth and S. M. Koushiappas, *Phys. Rev. D* **86**, 021302 (2012) [arXiv:1206.0796 [astro-ph.HE]].
 - [6] M. N. Mazziotta, F. Loparco, F. de Palma and N. Giglietto, arXiv:1203.6731 [astro-ph.IM].
 - [7] A. N. Baushev, S. Federici and M. Pohl, *Phys. Rev. D* **86**, 063521 (2012) [arXiv:1205.3620 [astro-ph.HE]].
 - [8] X. -Y. Huang, Q. Yuan, P. -F. Yin, X. -J. Bi and X. -L. Chen, *JCAP* **1211**, 048 (2012) [arXiv:1208.0267 [astro-ph.HE]].
 - [9] [Fermi-LAT Collaboration], *Astrophys. J. Suppl.* **199**, 31 (2012) [arXiv:1108.1435 [astro-ph.HE]].
 - [10] P. Salucci, M. I. Wilkinson, M. G. Walker, G. F. Gilmore, E. K. Grebel, A. Koch, C. F. Martins and R. F. G. Wyse, *Mon. Not. Roy. Astron. Soc.* **420**, 2034 (2012) [arXiv:1111.1165 [astro-ph.CO]].
 - [11] A. Charbonnier, C. Combet, M. Daniel, S. Funk, J. A. Hinton, D. Maurin, C. Power and J. I. Read *et al.*, *Mon. Not. Roy. Astron. Soc.* **418**, 1526 (2011) [arXiv:1104.0412 [astro-ph.HE]].
 - [12] W. A. Rolke, A. M. Lopez and J. Conrad, *Nucl. Instrum. Meth. A* **551**, 493 (2005) [physics/0403059].
 - [13] A. Drlica-Wagner, *Fermi Symposium 2012*,
 - [14] J. -M. Zheng, Z. -H. Yu, J. -W. Shao, X. -J. Bi, Z. Li and H. -H. Zhang, *Nucl. Phys. B* **854**, 350 (2012) [arXiv:1012.2022 [hep-ph]].
 - [15] J. Goodman, M. Ibe, A. Rajaraman, W. Shepherd, T. M. P. Tait and H. -B. Yu, *Nucl. Phys. B* **844**, 55-68 (2011) [arXiv:1009.0008 [hep-ph]].
 - [16] K. Cheung, P. -Y. Tseng and T. -C. Yuan, *JCAP* **1106**, 023 (2011) [arXiv:1104.5329 [hep-ph]].
 - [17] Z. -H. Yu, J. -M. Zheng, X. -J. Bi, Z. Li, D. -X. Yao and H. -H. Zhang, arXiv:1112.6052 [hep-ph].
 - [18] K. Cheung, P. -Y. Tseng, Y. -L. S. Tsai and T. -C. Yuan, *JCAP* **1205**, 001 (2012) [arXiv:1201.3402 [hep-ph]].
 - [19] Y. Mambrini, M. H. G. Tytgat, G. Zaharijas and B. Zaldivar, *JCAP* **1211**, 038 (2012) [arXiv:1206.2352 [hep-ph]].
 - [20] L. Bergstrom, T. Bringmann and J. Edsjo, *Phys. Rev. D* **83**, 045024 (2011) [arXiv:1011.4514 [hep-ph]].
 - [21] R. C. Cotta, A. Drlica-Wagner, S. Murgia, E. D. Bloom, J. L. Hewett and T. G. Rizzo, *JCAP* **1204**, 016 (2012) [arXiv:1111.2604 [hep-ph]].
 - [22] P. Scott, J. Conrad, J. Edsjo, L. Bergstrom, C. Farnier and Y. Akrami, *JCAP* **1001**, 031 (2010) [arXiv:0909.3300 [astro-ph.CO]].
 - [23] L. Roszkowski, E. M. Sessolo and Y. -L. S. Tsai, *Phys. Rev. D* **86**, 095005 (2012) [arXiv:1202.1503 [hep-ph]].
 - [24] S. Chatrchyan *et al.* [CMS Collaboration], *Phys. Lett. B* **716**, 30 (2012) [arXiv:1207.7235 [hep-ex]].
 - [25] G. Aad *et al.* [ATLAS Collaboration], *Phys. Lett. B* **716**, 1 (2012) [arXiv:1207.7214 [hep-ex]].
 - [26] <http://projects.hepforge.org/multinest/>
 - [27] K. Kowalska, S. Munir, L. Roszkowski, E. M. Sessolo, S. Trojanowski and Y. -L. S. Tsai, arXiv:1211.1693 [hep-ph].
 - [28] P. Bechtle, O. Brein, S. Heinemeyer, G. Weiglein and K. E. Williams, *Comput. Phys. Commun.* **182**, 2605 (2011) [arXiv:1102.1898 [hep-ph]].
 - [29] P. Gondolo, J. Edsjo, P. Ullio, L. Bergstrom, M. Schelke and E. A. Baltz, *JCAP* **0407**, 008 (2004) [arXiv:astro-ph/0406204].
 - [30] M. Cirelli, A. Strumia and M. Tamburini, *Nucl. Phys. B* **787**, 152 (2007) [arXiv:0706.4071 [hep-ph]].
 - [31] J. Hisano, S. Matsumoto, M. M. Nojiri and O. Saito, *Phys. Rev. D* **71**, 063528 (2005). [arXiv:hep-ph/0412403].
 - [32] A. Hryczuk, R. Iengo and P. Ullio, *JHEP* **1103**, 069 (2011) [arXiv:1010.2172 [hep-ph]].
 - [33] T. Sjostrand, S. Mrenna and P. Skands, *JHEP* **0605**, 026 (2006). [arXiv:hep-ph/0603175].
 - [34] T. Sjostrand, S. Mrenna and P. Z. Skands, *Comput. Phys. Commun.* **178**, 852 (2008) [arXiv:0710.3820 [hep-ph]].
 - [35] G. Corcella, I. G. Knowles, G. Marchesini, S. Moretti, K. Odagiri, P. Richardson, M. H. Seymour and B. R. Webber, *JHEP* **0101**, 010 (2001) [hep-ph/0011363].
 - [36] E. Aprile *et al.* [XENON100 Collaboration], *Phys. Rev. Lett.* **109**, 181301 (2012) [arXiv:1207.5988 [astro-ph.CO]].
 - [37] http://cosmology.bao.ac.cn/~huangxy/GetLdSphs_v1.tar.gz